Journal of The Electrochemical Society

The Electrochemical Society
Advancing solid state & electrochemical science & technology

OPEN ACCESS

Combinatorial Studies into the Effect of Thermally Inter-Diffused Magnesium on the Kinetics of Organic Coating Cathodic Delamination from Zinc Galvanized Steel

To cite this article: N. Wint *et al* 2020 *J. Electrochem. Soc.* **167** 021502

Journal of The Electrochemical Society, 2020 **167** 021502

Combinatorial Studies into the Effect of Thermally Inter-Diffused Magnesium on the Kinetics of Organic Coating Cathodic Delamination from Zinc Galvanized Steel

N. Wint,*,z Z. S. Barrett, H. N. McMurray,* and G. Williams

Materials Research Centre, College of Engineering, Swansea University, Bay Campus, Fabian Way, Crymlyn Burrow, Swansea, SA1 8EN, United Kingdom

This paper describes a high-throughput study into the role of Mg in preventing corrosion driven coating disbondment of organic coatings from Zn-Mg alloy galvanized steel. A graded Mg wedge is applied to a hot-dip zinc galvanised steel substrate using physical vapour deposition, and subsequently annealed to produce metallic inter-diffusion and formation of Mg_2Zn_{11} intermetallic. An overcoat of electrically insulating polyvinyl butyral (PVB) is applied and corrosion is initiated from a penetrative coating defect using an aqueous electrolyte. The variation in Mg coating weight across the wedge facilitates a systematic investigation of the effect of Mg on Volta potential and the rate of corrosion driven cathodic coating disbondment using scanning Kelvin probe (SKP) potentiometry. The rate of cathodic disbondment is shown to decrease rapidly even at very low Mg coating weight (corresponding to 25 nm thickness before annealing). The results are explained in terms of the galvanic polarity of the corrosion cell formed between Zn exposed at the defect site, and the intact Zn-Mg layer at the metal-organic coating interface.
 [DOI: 10.1149/1945-7111/ab6289]

Manuscript submitted October 21, 2019; revised manuscript received December 12, 2019. Published January 9, 2020.

Magnesium is increasingly used as an alloying element in zinc-based galvanized coatings applied to steel substrates intended for architectural and automotive applications.[1–4] In such applications the galvanized surface is typically overcoated with an organic film (paint, lacquer or laminate).[1–4] Failure via corrosion-driven organic coating disbondment is therefore a problem of particular interest.[1–4] The current paper focuses on one important mode by which such corrosion-driven failure can occur, namely cathodic delamination. In the case of cathodic delamination it is the cathodic oxygen reduction reaction (ORR) which is responsible for the disbondment of the organic coating from the metal substrate. Anodic metal dissolution occurring in the defect region is coupled to a cathodic delamination front via a thin (<5 μm) gel like film of electrolyte which ingresses beneath the coating.[5–7] In the delaminated region, the potential increases as a function of distance away from the artificial defect, and the potential difference between this region and that of the intact coating (higher potential) creates a driving force for cation migration away from the defect region and beneath the organic coating.[7] Cathodic delamination is known to affect conventional organic coated zinc galvanized steel.[8–10] However, it has been reported that magnesium additions, present in the form of the intermetallic (IM) compound $MgZn_2$, can act to profoundly decrease cathodic delamination rates.[1–4] For these reasons, the principal aim of the work to be presented here was to systematically characterize the relationship between magnesium content and rates of cathodic organic coating delamination from galvanized steel. In so doing a combinatorial metrology for obtaining such a characterization has been developed.

High-throughput (combinatorial) metrologies have evolved over the past few decades as a useful alternative to the traditional "one-composition-at-a-time" approach for rapidly determining composition-structure-property relationships in novel materials systems.[11–13] For such determinations, a combinatorial library, typically a continuous composition-spread film, is first synthesized and then characterized using high throughput measurement techniques for selected properties of interest. Thus, two essential tools are required for a combinatorial approach: the first a means of synthesizing the composition spread library film, and the second a high-throughput measurement technique for screening the desired property or characteristic.

Zinc-magnesium alloy coatings are typically applied to the steel substrate by hot dipping.[1,14] However, such an approach does not readily permit the rapid development of a combinatorial library of continuously varied alloy composition. One recognized methodology for so doing involves the deposition of metallic films via a sputtering route.[11–13] For example, simultaneous co-deposition using two or more sputtering targets can (in principle) directly create a continuous composition spread library on a single substrate. Alternatively, individual sputtering targets can be used in conjunction with a movable shutter to deposit a graded metal layer or "wedge" (shown schematically in Fig. 1a) of continuously varied thickness.[13,15,16] By superimposing wedges of dissimilar metals, and then annealing to produce thermal interdiffusion, a single-substrate combinatorial library of alloy composition can once again be created.

Physical vapor deposition (PVD) has been widely used as a sputtering technique for the deposition of metallic coatings.[17–21] Furthermore, it has been demonstrated that magnesium layers, deposited onto a pre-existing galvanized steel substrate using PVD, may subsequently be thermally interdiffused by annealing to produce Zn-Mg coatings.[20] It has thus been shown that, for annealing temperatures between 300 °C and 400 °C, the principal products of interdiffusion are the crystalline IM compounds $MgZn_2$ and Mg_2Zn_{11}, which tend to form in bands or layers parallel with the basal plane of the coating. However, if an electrogalvanized steel (where the original coating is a pure zinc electrodeposit) is used as the substrate, results may be complicated by thermal diffusion of iron from the underlying steel into the Zn-Mg coating at higher annealing temperatures.[21,22]

Given the above, it was decided to use PVD in conjunction with a movable shutter to deposit wedges of magnesium metal onto a pre-existing galvanized steel substrate and then induce thermal interdiffusion by annealing. In so doing, the intention was to generate continuously varied, single-substrate, combinatorial libraries corresponding to zinc-rich portions of the zinc-magnesium binary diagram. One important drawback of this approach is that the layered structure of the interdiffused Zn-(PVD)Mg coatings (which from this point will be referred to as ZM coatings) does not strongly resemble the microstructure evolving in hot-dipped Zn-Mg or Zn-Al-Mg alloy coatings. Nevertheless, it would seem entirely appropriate as a means of determining how varying quantities of Mg-Zn IM, present at the metal surface, affects the tendency of an organic overcoat to undergo cathodic disbondment. Hot-dip galvanized steel, produced using a zinc spelter which also contains 0.15 wt% aluminium, was used as the substrate. The small aluminium addition acts to block iron-coating interdiffusion through the formation of a crystalline aluminium-rich IM layer (nominal composition $((Zn,Al)_5Fe$) at the coating-steel interface.[23]

*Electrochemical Society Member.
zE-mail: n.wint@swansea.ac.uk

The high-throughput measurement technique selected as a means of characterizing the ZM coated combinatorial library samples with respect to cathodic delamination resistance involves the Scanning Kelvin Probe (SKP). SKP has been widely used as means of following the progress of organic coating delamination from a variety of metallic substrates,[6–10,15,24,25] including galvanized steel[8–10] and pure phase $MgZn_2$,[1–4] and recent work has highlighted its role in providing mechanistic information by measuring the characteristic potentials associated with different portions of a localized corrosion cell.[26] Thus, the high cathodic delamination resistance observed in the case of organic coated $MgZn_2$ has been attributed to an inversion in the normal polarity of the localized corrosion cell evolving between an intact organic-coated surface and $MgZn_2$ exposed at a penetrative organic coating defect.[1–4] Here we show that, by arranging the geometry of the localized corrosion cell in such a way that cathodic delamination occurs in a direction normal to the gradient of the original (PVD)Mg wedge deposit, it is possible to characterize simultaneously the full range of Mg coating weights present in a single-substrate combinatorial library. An exactly similar approach has been reported previously for PVD aluminium wedge deposits on iron.[15,16]

Experimental

Materials.—Hot dip galvanized steel was obtained from Tata Steel UK and consisted of 0.8 mm thick mild steel coated with 20 μm layer zinc (containing 0.15 wt% Al) on each side. Mg deposition sources were acquired from Kurt J Lesker and were of at least 99.95% purity. All chemicals, including polyvinyl butyral-co-vinyl alcohol-co-vinylacetate (PVB) (molecular weight 70 000–-100 000 Da) were of analytical grade purity and supplied by Sigma Aldrich Chemical Company.

Methods.—Galvanized steel coupons of approximately 35 mm × 50 mm were cut from larger sheets and 5 μm abrasive alumina powder (Buehler) was used to remove any surface contamination. The coupons were then rinsed using distilled water and ethanol, and subjected to both an ultrasonic acetone and ethanol wash (each wash lasted 10 min). Coupons were finally rinsed with ethanol and dried using pressurized air.

Application of Mg PVD film.—A Kurt J Lesker PVD75 Physical Vapour Deposition (PVD) system was used to apply thin Mg layers onto the cleaned zinc coated steel surface, following a procedure described previously.[15] Coupons were attached to the stainless steel holder via four screws to ensure that they remained flat once loaded into the deposition chamber. An area of the coupon, on to which deposition would take place, was exposed (shown schematically in the first image of Fig. 1b) using vacuum compatible polyimide tape (CHR K250 Saint-Gobain Performance Plastics). The holder was then loaded into the vacuum chamber of the PVD system in a position where it could not obstruct the sliding shutter mechanism (used to apply films of variable thickness). Before deposition of the Mg film, the surface of the coupon was plasma etched for 15 min in an argon atmosphere. An argon gas flow rate of 140 standard cubic centimetres per minute and an applied power density of 15 $W \cdot cm^{-2}$.

Deposition of the Mg film took place within the same chamber, which was maintained at a pressure of at 3×10^{-3} Torr (the base pressure of the vacuum pump was 5×10^{-8} Torr). Deposition was carried out onto the shutter for the first 5 min to ensure stabilization of the deposition rate and to avoid depositing surface oxide from the target. A Mg film, varying linearly in thickness, was then deposited onto the un-taped area. Prior to deposition, the shutter was positioned such to cover the entire exposed area (shown

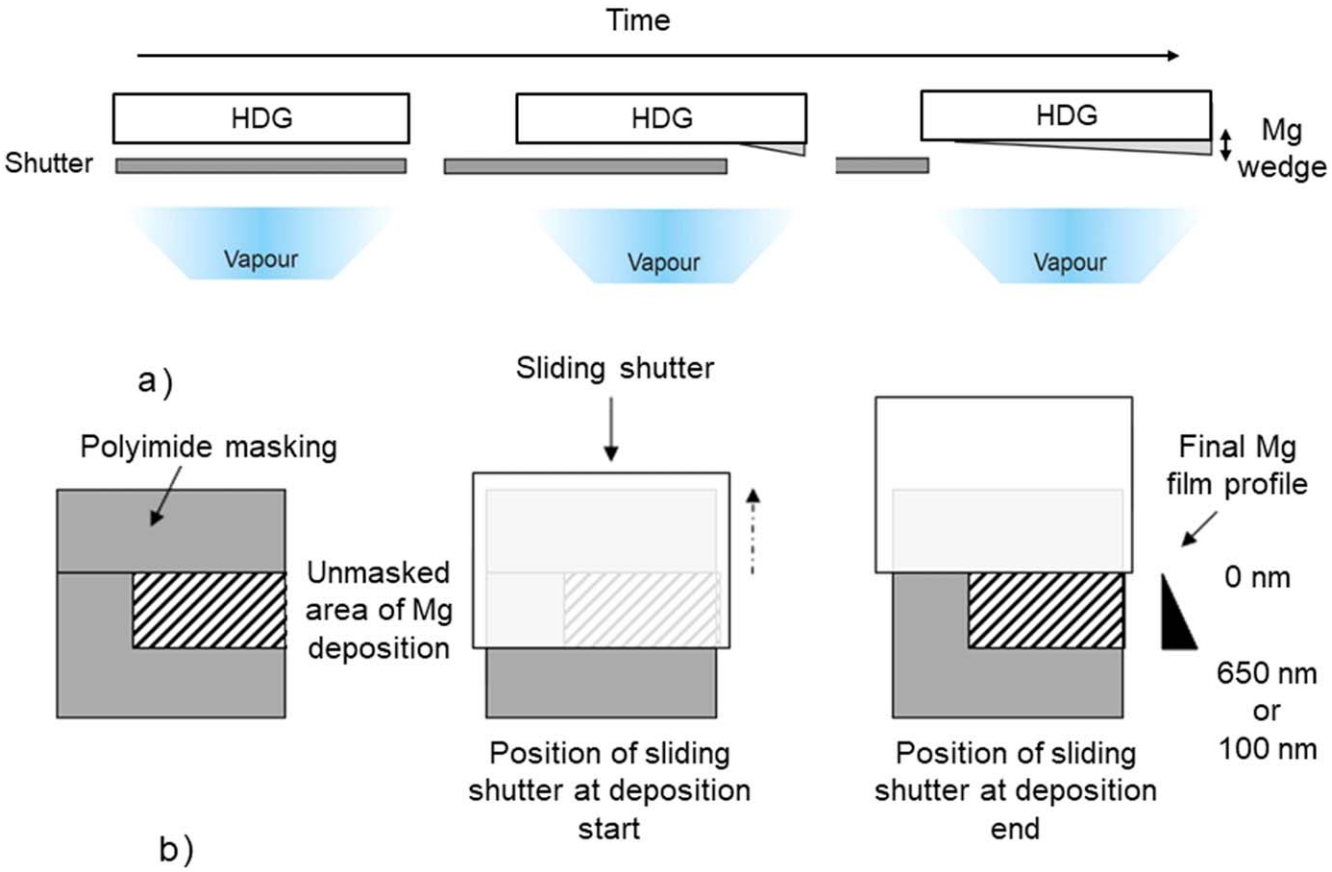

Figure 1. A schematic representation of the process by which a graded wedge coating is formed using a sliding shutter mechanism and the finished wedge coating produced in the case of an Mg coating.

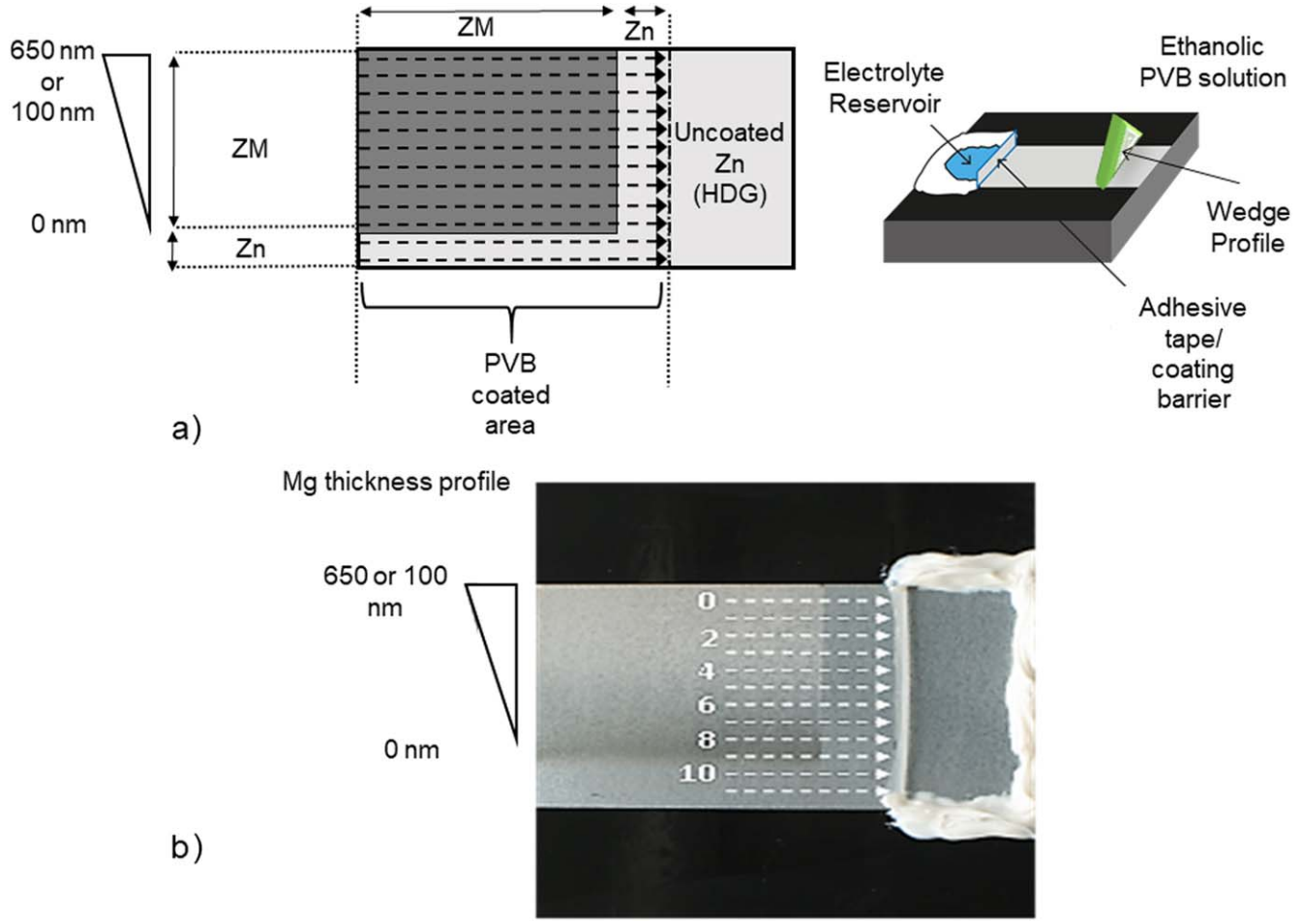

Figure 2. (a) A schematic and (b) a photograph of a Stratmann delamination cell showing the orientation of the inter-diffused Mg wedge and direction of scan which meant that each scan line followed the progress of the PVB delaminating from ZM alloys of different compositions.

schematically in first image of Fig. 1a and second image of Fig. 1b). The rate of shutter withdrawal was used to control the rate at which the film thickness was varied, following Eq. 1, where v is the shutter speed, w is the width of the area to be coated, T is the maximum film thickness required, and D is the deposition rate.

$$v = \frac{w}{T/D} \quad [1]$$

Deposition was stopped at the point where all of the un-masked area was exposed. The argon gas flow rate used was 40 SSCM and the power was 150 W. A deposition rate of $\sim$4.9 Å $\cdot$ s^{-1} was achieved throughout. All coating thicknesses were monitored indirectly using a Sigma Instruments oscillating crystal (calibrated for the physical properties of the coating). For single thickness films (used for both GDOES and XRD measurements) the same methodology was followed with the exception that the sliding shutter was not used.

Magnesium film inter-diffusion.—Following Mg deposition, the coupons were taken out of the PVD chamber. Any tape (used to mask areas of the coupon) was removed and they were then transferred to a Carbolite tube furnace (time between removal from PVD chamber and entering furnace $<$10 min). Coupons were heated to 340 °C, at which they were held for 10 min, before cooling.[21] An inert atmosphere was maintained throughout the period of the heating and cooling cycle by flowing argon gas at a rate of 1.5 l $\cdot$ min^{-1}. Coupon temperature was monitored using a K-type thermocouple which was spot welded to its rear face.

GDOES; Depth profiling of the inter-diffused films were performed using a Horiba-Jobin Yvon-5000RF glow discharge optical emission spectroscopy (GDOES) unit.

XRD; Data were collected on a Bruker C2 Gadds with a 1.6 kW (40 kV, 40 mA) Cu sealed tube generator equipped with a single Goebel mirror (0.5 mm collimator), a xyz stage and 2D multi-wire HiStar detector. A single 2D image was acquired for 600 s. Data were corrected for spatial distortion and integrated in Chi. Analysis was undertaken using reference data from PDF-2 (2002) International Centre for Diffraction Data.

Cathodic disbondment studies.—A "Stratmann" type cell (shown in Fig. 2) was used to investigate the influence of influence of Mg on the rate of corrosion driven cathodic delamination.[6–10,15,24,25] A strip of clear adhesive tape was applied across one end of a coupon in such a way that it ran parallel to the profile of the coating wedge. Insulating tape was attached onto the two parallel sides of the coupon which ran perpendicular to the clear adhesive tape. The remaining area was coated in an ethanolic solution (15.5 wt%) of PVB via bar casting. The insulating tape acted as a height guide and the dry film thickness (measured using a micrometer screw gauge) was 30 μm. A 15 mm $\times$ 20 mm area of bare metal was exposed by partially peeling back the clear tape. The residual clear tape and PVB overcoating acted as a barrier between the intact PVB coating and the exposed metal "defect" area. Non-corrosive silicone rubber was used to line the remaining sides of the defect, to which a 2 cm^3 volume of 0.86 M aqueous NaCl electrolyte was applied to initiate corrosion.

Figure 2a shows a schematic version of the delamination cell arrangement indicating the various Mg alloyed (ZM), unalloyed Zn (HDG), PVB coated and uncoated regions of the cell. Figure 2b shows the PVB (30 μm) coated samples as part of the delamination cell arrangement prior to introduction of the 0.86 M NaCl

experimental electrolyte. It may be appreciated by Figs. 2a and 2b that the ZM portion of the metal substrate surface does not extend to the lip of the PVB coated area. Thus, any process of cathodic PVB disbondment will become initiated at the Mg-free Zn (HDG) metal-PVB interface and must propagate for a distance of ~4 mm before encountering the ZM-PVB interface.

The reason for choosing to adopt such an arrangement were two-fold; 1.) by allowing initiation to occur on Zn we de-convolve the effects of Mg on the initiation and propagation of cathodic disbondment. By so doing we exclude the possibility that Mg is simply acting to reduce the probability of disbondment becoming initiated and not to inhibit subsequent disondment kinetics. 2.) Once established, the polarity of the cathodic disbondment cell disfavours migration of Cl^- ions beneath the disbonded organic films. Exclusion of Cl^- minimizes the tendency for anodic Mg dissolution to occur. The effect of Mg on cathodic disbondment kinetics may therefore be quantified in isolation without the risk of complication from anodic undercutting processes.

Calibration of the SKP was completed to obtain a relationship between the Volta potential value (as recorded by the SKP) and the corrosion potential (E_{corr}) associated with the polymer covered metal.[6,9] Ag/Ag^+, Cu/Cu^{2+}, Fe/Fe^{2+} and Zn/Zn^{2+} couples were used to complete the calibration process following a procedure established previously.[6,9] Each of the metals was machined into a disc (15 mm diameter, 5 mm thick) within which a well (1 mm deep wells of 8 mm diameter) was formed. 0.5 M aqueous solutions of the respective metal chloride salt (0.5 M nitrate salt in the case of Ag) were used to fill the well. The metal electrode potential was simultaneously measured vs SCE using a Solartron 1280 potentiostat and compared to the Volta potential difference measured above the filled well by the SKP.

A constant humidity of *ca.* 95% RH was achieved by placing reservoirs of 0.86 M aqueous NaCl (pH 6.5) within the SKP chamber. The temperature was maintained at 25 °C. The SKP gold wire probe (125 μm diameter) was positioned at a constant height of 100 μm above the sample and scanned along twelve 12 mm long lines, perpendicular and contiguous to the defect/coating interface. Given the orientation of the inter-diffused Mg wedge, scanning in this manner meant that each scan line followed the progress of the PVB delaminating from ZM alloys of different compositions (see Fig. 2b). The number of scan lines was chosen so as to maximise the amount of Mg thickness values whilst ensuring that the distance between lines was greater than the lateral resolution L of the SKP (given by Eq. 2) where d is probe-specimen distance and D is the probe diameter.[27]

$$L = 0.884\, d + 0.4\, D \qquad [2]$$

Using Eq. 2 it can be shown that in the case that $d = 100$ μm and $D = 125$ μm, the lateral resolution will be ~140 μm. For the case that the inter line spacing was greater than 140 μm, Volta potential values recorded for each scan line were not influenced by the adjacent scan line (for which Mg thickness would be substantially different).

Scanning took place immediately following the application of the electrolyte to the defect. Subsequent scans took place at intervals of 1 h for a total of up to 48 h. 20 E_{corr} values were recorded per mm. In some cases E_{corr} profiles, made noisy by the nature of the interdiffused ZM layer, were smoothed in Origin software using a Savitzky Golay method whereby successive sub-sets of 20 adjacent data points were fitted with a second degree polynomial by the method of linear least squares. This process was completed to reduce the complexity of the profiles and to aid in determining the location of the cathodic delamination front.

Results and Discussion

Structural/compositional characteristics.—Figure 2b shows the appearance of the combinatorial ZM wedge sample immediately after thermal inter-diffusion of HDG and a 600 nm thick Mg wedge, and prior to over-coating with PVB. The unalloyed HDG surface is visibly polycrystalline. By contrast, the thermally inter-diffused ZM in the thicker portion of the ZM region appears significantly more uniform, light grey in colouration, with no surface crystallinity resolvable by eye. Towards the thinner edge of the wedge the ZM coating, to some extent, follows the topography of the substrate allowing the polycrystalline morphology of the HDG to become visible. Figure 3 shows an SEM cross section through the ZM layer for the case that the Mg layer thickness prior to inter-diffusion was 600 nm. The ZM layer is somewhat uneven, reflecting the uneven HDG substrate surface, and varies in thickness between 1 and 2 μm. Two layers are visible in the interdiffused ZM coating. Entirely similar results have been reported by other authors using PVD and thermal inter-diffusion and attributed it to the formation of $MgZn_2$ (upper layer) and Mg_2Zn_{11} (lower layer).[21,22] However, Figure 4 shows a GDOES depth profile derived from a ZM surface produced by the thermal inter-diffusion of a 600 nm Mg layer, and the near surface Mg concentration is 8 wt%, consistent with the presence of Mg_2Zn_{11}. Furthermore, a glancing angle XRD spectrum, obtained from an exactly similar sample surface and shown in Fig. 5, again indicates the presence of crystalline Mg_2Zn_{11} but not $MgZn_2$. The various peaks in Fig. 5 are labelled in accordance with reference data from PDF-2 (2002) International Centre for Diffraction Data. Thus, if any $MgZn_2$ is present in the interdiffused coating it is not present in sufficient quantities to be evident in either the XRD or GDOES data.

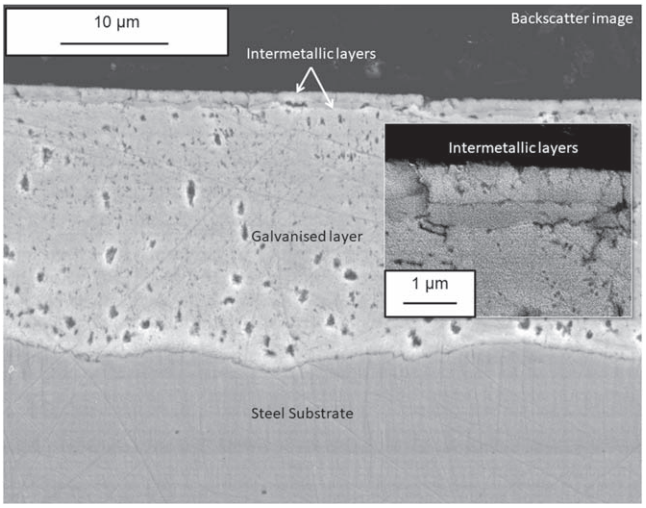

Figure 3. SEM cross section through the ZM layer over a portion of the surface where the Mg layer prior to inter-diffusion had been 600 nm.

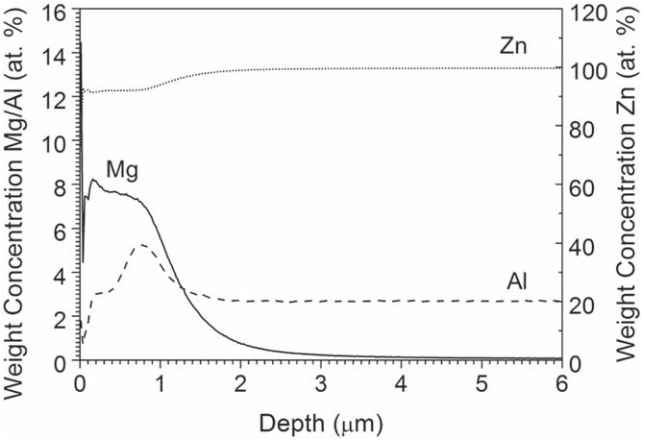

Figure 4. A GDOES depth profile derived from a ZM surface produced by the thermal inter-diffusion of a Mg layer.

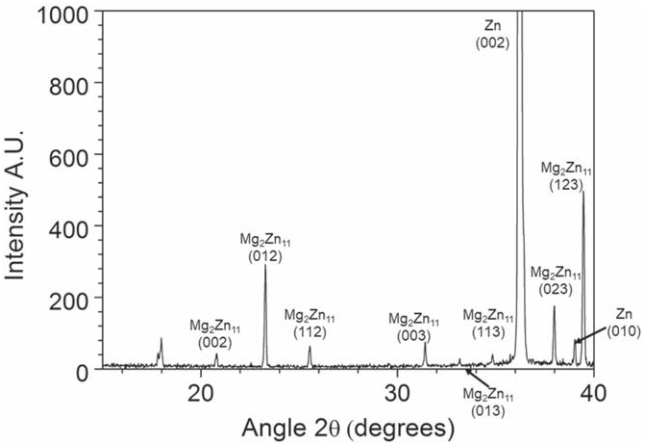

Figure 5. An XRD spectrum derived from a ZM surface produced by the thermal inter-diffusion of a Mg layer.

SKP potentiometry.—The effect of Mg film thickness (d) upon the E_{corr} values for inter-diffused ZM films over-coated with 30 μm PVB was quantified during initial experiments. The meaning of E_{intact} (in the context of a metal coated with a non-conducting polymer) has been explained in detail previously,[24] and reflects the open circuit potential of the oxide-covered metal substrate. Figure 6a shows a profile of E_{intact} as a function of initial Mg layer thickness. Measurements were obtained using SKP in humidity (~96% RH) air prior to the introduction of 0.86 M NaCl delamination electrolyte. Values shown are based on the average of all readings taken at each thickness and error intervals represent one standard deviation on the mean. The local E_{intact} values vary with the thickness of the initial (pre inter-diffusion) Mg-layer. Mg-free, Zn (HDG) portions of the sample exhibit E_{intact} of ~ -0.3 V vs SHE i.e. similar to values reported previously for PVB coated HDG.[8,9,25] The potential value remains constant for Mg thickness values $\geqslant$100 nm and $\leqslant$400 nm. A decrease in potential (of up to ~0.3 V) is observed for Mg thickness values $\geqslant$400 nm. This finding would suggest that the outer surface of the inter-diffused ZM layer is becoming enriched in Mg for higher (initial) Mg thickness. There is no evidence from XRD (Fig. 5) for the formation of $MgZn_2$ under these circumstances. However, it has been proposed that ZM intermetallic compounds may exhibit some degree of variable stoichiometry.[28]

The observed variation in Volta potential ($\Delta\Psi$) values, with original Mg film thickness in Fig. 6a is most readily explained on the basis of a contact potential developing between the HDG zinc substrate and superposed MgZn IM layer(s). The Volta potential difference (or contact potential) established between the Zn and the overlying ZM layer is ~0.75 eV and is a result of their varying work functions (W). When two dissimilar, electronically conducting materials are connected together (in such a way that electrons can be transported between them) they will share a common Fermi level and the Volta potential difference between them can be calculated using Eq. 3.

$$\Delta\Psi_1^2(eV) = W_1 - W_2 \qquad [3]$$

By using Eq. 3, in conjunction with the value of $\Delta\Psi_1^2$ (in this case 0.75 eV) and a literature value for the work function of polycystalline zinc ~4.3 eV[29] (which best reflects the condition of metal coupons used), it is possible to calculate the work function of Mg_2Zn_{11} to be 3.6 eV. It should be noted, firstly, that both the presence of an oxide layer and/or trace contamination can have an effect on metallic work functions by up to 0.2 eV,[3] and secondly that the literature values of zinc work function are highly variable. Despite this, the calculated value is expected to be a reasonable reflection of the true value. As far as the authors are aware, the work function of Mg_2Zn_{11} has not been published previously. However, the value of 3.6 eV calculated for Mg_2Zn_{11} would seem reasonable as a first attempt, given that it falls below the value widely adopted for pure Zn (~4.33 eV)[29] and is more consistent with that of pure Mg (~3.68 eV).[30]

The variation in E_{intact} with Mg layer thickness is more significant for initial (pre-inter-diffusion) Mg film thicknesses less than 100 nm than for thicknesses between ~150 nm and ~450 nm (Fig. 6). The value of E_{intact} recorded decreases from (-0.3 ± 0.05) V vs SHE (similar to values reported previously for PVB coated HDG[8,9,25]) to (-0.8 ± 0.1) V vs SHE as Mg layer thickness values increase from 0 nm to 70 nm. This decrease in potential can be seen more clearly in Fig. 7, which shows E_{intact} as a function of initial Mg layer thickness for a 100 nm wedge. The value of E_{intact} decreases almost linearly from (-0.3 ± 0.02) V vs SHE to (-0.6 ± 0.1) V vs SHE for thicknesses between 0 nm and 70 nm. It seems reasonable

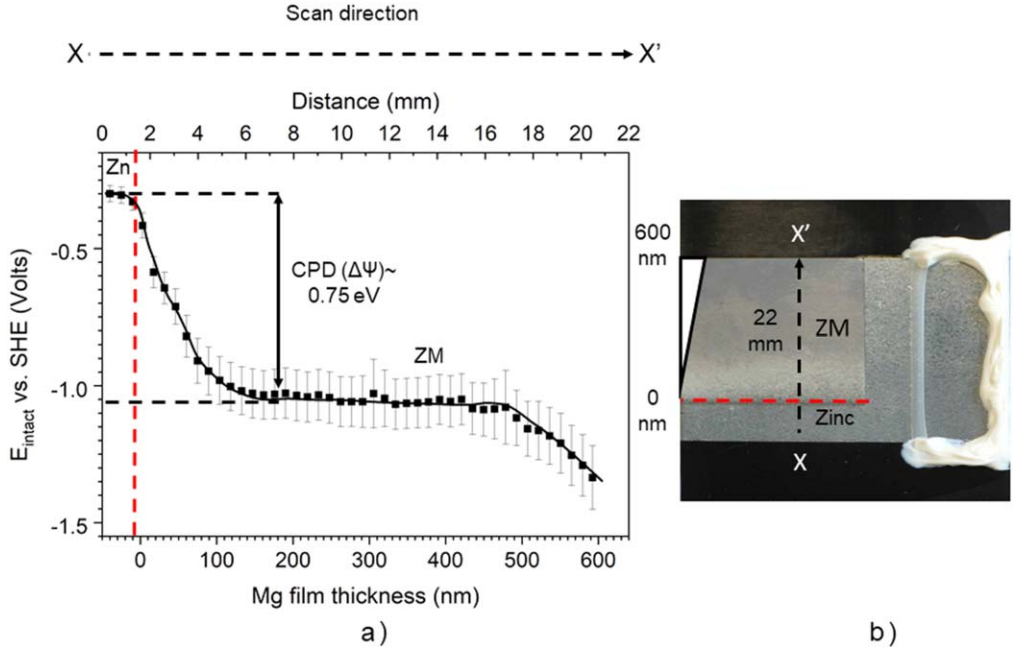

Figure 6. SKP derived E_{intact} values as a function of pre inter-diffusion Mg layer thickness for a PVB coated 600 nm PVD ZM wedge.

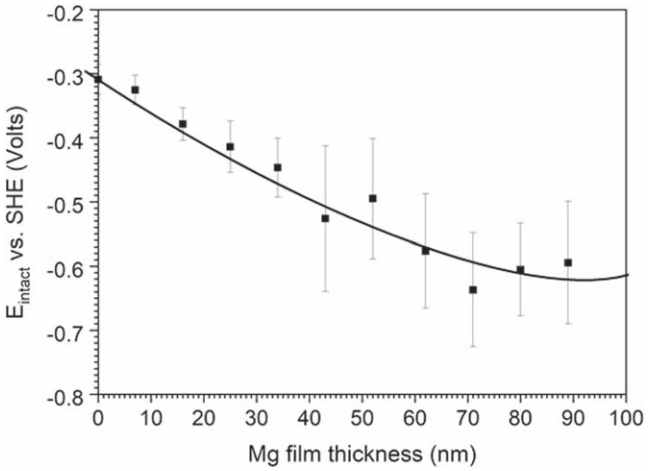

Figure 7. SKP derived E_{intact} values as a function of pre inter-diffusion Mg layer thickness for a PVB coated 100 nm PVD ZM wedge.

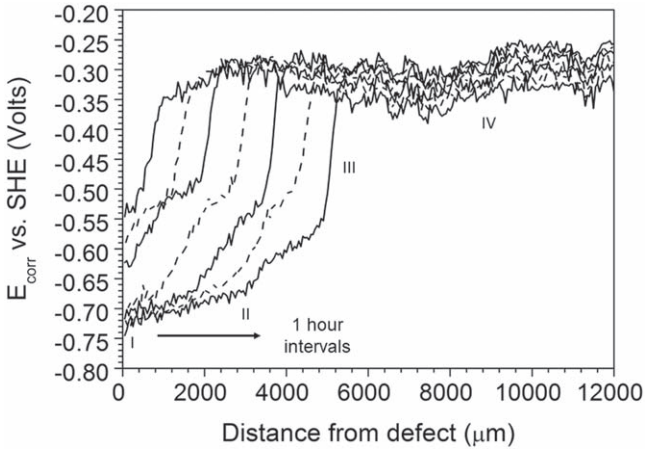

Figure 8. SKP derived E_{corr} as a function of distance from defect *(x)* profiles recorded for the delamination of a PVB model coating from HDG after initiation using a 0.86 M NaCl electrolyte.

to assume that a less complete ZM layer is produced at these reduced thicknesses and that E_{intact} tends toward that of the underlying HDG substrate.

Cathodic delamination studies.—*Unmodified HDG;* Baseline delamination kinetics were obtained for the cathodic disbondment of PVB from a plain HDG substrate. When cathodic disbondment occurred on the unmodified HDG substrate a series of time-dependent $E_{corr}(x)$ profiles were obtained as shown in Fig. 8. The significance of these profiles has been described at length elsewhere and will be dealt with here only briefly.[8–10] Initially, the potential value associated with the intact PVB coated Zn surface (E_{intact}) corresponds to a "passive" state (∼−0.3 V vs SHE) and is determined by the relative rates of anodic zinc dissolution (Eq. 4) and the ORR (Eq. 6).[8–10] The rate of the anodic reaction is slowed by the presence of the zinc hydr(oxide) layer whilst the permeability of the PVB layer means that the ORR is kinetically faster.

Upon contact with the NaCl electrolyte (∼pH 6.5), the zinc hydr (oxide) layer dissolves and Zn undergoes anodic dissolution via Eq. 4. The potential within the near defect region (I) falls to values corresponding to actively corroding Zn (∼−0.7 V vs SHE) following Eq. 5.[8–10] The sharp transition between the defect and intact coating (IV) is referred to as the delamination front (III) and can be seen in the profiles in Fig. 8. These profiles can be understood as a galvanic cell within which the defect is the principal anodic site and

Table I. PVD Mg film thickness associated with each SKP scan line.

Scan line	PVD Mg Thickness prior to inter-diffusion (nm)	
	600 nm wedge	100 nm wedge
0	588	89
1	526	80
2	464	71
3	402	62
4	340	52
5	279	43
6	217	34
7	155	25
8	93	16
9	31	7
10	0	0
11	0	0

is coupled to region IV. This galvanic coupling results in an anodic potential shift at the defect and a cathodic potential shift at the metal/coating interface and is facilitated by an ionic current flux which passes through the underfilm electrolyte as delamination proceeds (Region II).

$$Zn_{(s)} \leftrightarrow Zn^{2+}_{(aq)} + 2e^- \quad [4]$$

$$E_{eq} = -0.763 + 0.0295 \log [Zn^{2+}] \quad [5]$$

$$O_2 + 2H_2O + 4e^- \leftrightarrow 4OH^-_{(aq)} \quad [6]$$

$$E_{eq} = 1.228 - 0.0591pH + 0.0147 \log pO_2 \quad [7]$$

Although anodic dissolution is initially constrained to the defect region, the elevated pH (pH 10-11) encountered within the disbonded region results in the dissolution of the surface zinc hydr (oxide) to soluble hydrogen zincate (Eq. 8) or zincate (Eq. 9).[9,10]

$$Zn(OH)_2 \leftrightarrow HZnO^-_{2(aq)} + H^+_{(aq)} \quad [8]$$

$$Zn(OH)_2 \leftrightarrow ZnO^-_{2(\boldsymbol{aq})} + 2H^+_{(\boldsymbol{aq})} \quad [9]$$

At pH values greater than 10.37 the zinc uncovered can dissolve via Eq. 10.[9,10]

$$Zn_{(s)} + 2H_2O \leftrightarrow HZnO^-_{2(aq)} + 3H^+_{(aq)} + 2e^- \leftrightarrow \quad [10]$$

$$E_0 = 0.441 - 0.1182pH + 0.0295 \log (ZnO_2^{--}) \quad [11]$$

A sharp inflection in potential values is seen to move from left to right (in Fig. 8) as delamination proceeds. The point of maximum slope $\left(\frac{dE}{dx}\right)$ is taken as a semi-empirical indicator of the delamination front. The time dependent distance of the front from the artificial defect (x_{del}) can therefore be monitored easily and is plotted as a function of the associated delamination time (t_{del}) to obtain kinetic data. For unpigmented coatings, it is the migration of electrolyte cations (in this case Na^+) in the underfilm electrolyte, which typically controls the delamination rate.[7] Delamination kinetics are then predicted to be parabolic and to follow Eq. 12, where t_i is the time before initiation of corrosion-driven delamination and k_d is the parabolic delamination rate constant.

$$x_{del} = k_d (t_{del} - t_i)^{\frac{1}{2}} \quad [12]$$

600 nm *wedge;* A similar experiment was then conducted on a ZM wedge modified HDG sample for which the maximum Mg layer thickness, prior to inter-diffusion, was 600 nm. The thickness of the Mg layer at each point was calculated from the distance between each scan line and by assuming that there was a linear gradient in thickness across the wedge. The Mg layer thickness values

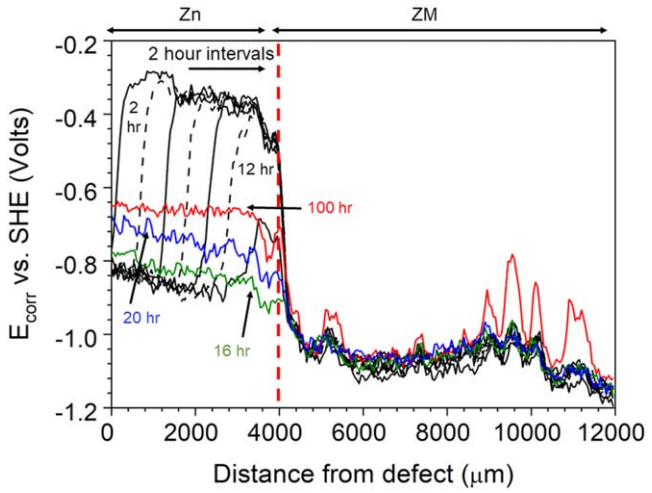

Figure 9. SKP derived E_{corr} as a function of distance from defect *(x)* profiles for the delamination of a PVB model coating from a ZM wedge coated HDG substrate after initiation using a 0.86 M NaCl electrolyte. The profile is taken from portions of the sample surface where the initial (pre-interdiffused) Mg layer thickness was 588 nm.

associated with each scan line are given in Table I. Figure 9 shows the time dependent $E_{corr}(x)$ profiles obtained for line 11 (588 nm Mg). In Fig. 9 it may be seen that, initially, E_{intact} values over the unmodified Zn portion (∼−0.3 V vs SHE) reflect those observed in Fig. 8. As delamination proceeds over the unmodified Zn surface E_{corr} *(x)* profiles evolve, which are, in the main entirely similar to Fig. 8. However, once the delamination front reaches the edge of ZM region no further propagation is observed. That is to say, no wave of potential variation is observed to move over the ZM surface. In comparison to Fig. 8, the E_{corr} recorded in the intact region is lower (∼−1.0 V vs SHE) than that recorded within the defect region (∼−0.75 V vs SHE). It would therefore seem reasonable to propose that, as with pure $MgZn_2$,[1–4,11] the lack of cathodic delamination observed in the case of Mg_2Zn_{11} or $MgZn_2$ (formed at a galvanized Zn surface) results from the galvanic polarity of the corrosion cell. SKP has previously been used to demonstrate the ability of $MgZn_2$ to resist cathodic coating delamination.[1–4,11] The $MgZn_2$ and Mg_2Zn_{11} IM phases formed within Zn-Mg and Zn-Al-Mg alloys have been shown to corrode sacrificially. The Mg^{2+} ions released can react with OH^- (produced at the cathode) to form $Mg(OH)_2$[3,14,15] and this process ensures that the surface pH is

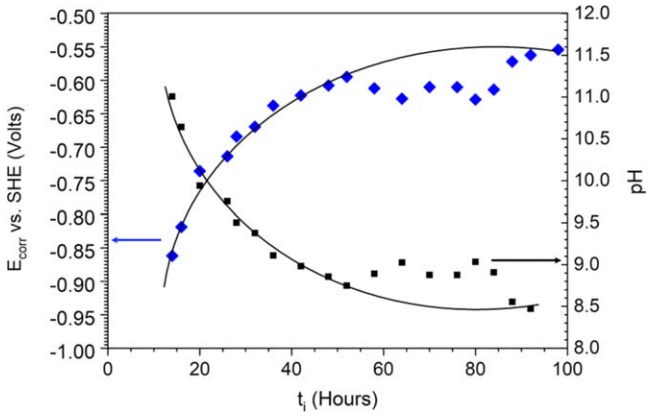

Figure 10. The mean value of E_{corr} and estimated underfilm pH in the delaminated region plotted as a function of time after the cessation of delamination of a PVB model coating from a ZM wedge coated HDG substrate after initiation using a 0.86 M NaCl electrolyte. The values are taken from portions of the sample surface where the initial (pre-interdiffused) Mg layer thickness was 588 nm.

maintained at values at which protective zinc hydr(oxides) are stable.[4,12] The selective dissolution which occurred in the defect region, meant that the defect potential increased to values of freely corroding zinc. The formation of a large band gap oxide at the intact $MgZn_2$/oxide/polymer interface resulted in increased cathodic polarization, and the galvanic polarity of the corrosion cell meant that cathodic delamination from the IM surface was completely inhibited.[1–4]

It is also evident from Fig. 9 that once the cathodic delamination front has reached the ZM portion of the coated sample, and the delamination rate has fallen to zero, potentials in the delaminated (zinc) portion of the sample start to rise. The mean value of E_{corr} in the delaminated region is plotted vs time in Fig. 10 which shows that E_{corr} increases from −0.82 V vs SHE (16 h) to −0.74 V vs SHE (20 h) over a period of 4 h after the cessation of delamination. If the measured values of E_{corr} are assumed to be close to the reversible potential for Zn oxidation (a cathodically controlled reaction), obtained via Eq. 10, and that the underfilm electrolyte is in isopiestic equilibrium with the reservoir electrolyte (0.86 M), a first approximation of the underfilm pH values can be made using Eq. 11. The implication here is that once OH^- production (through Eq. 6 at the delamination front) stops, underfilm pH moderates as OH^- is consumed. The further implication is that a significant fraction of total underfilm ORR occurs at the delamination front (as opposed to the portion of the sample where delamination has already occurred). This would be true if either i.) the underfilm electrolyte layer was acting as a barrier to O_2 mass transport and/or ii.) the corroded underfilm Zn surface was relatively inactive with respect to the ORR.

A question arises as to what extent the delaminated regions E_{corr} values recorded by the SKP, and shown in Fig. 9, actually reflect under-film pH. The accuracy with which Eq. 11 is able to predict the underfilm pH is dependent upon the degree to which polarization and ohmic effects distort the thermodynamic potential associated with the system. Whilst it is true that the ohmic contribution is unknown, there is no evidence of a potential gradient developing between the anode and cathode shown in Fig. 9. This finding is consistent with the cessation of the cathodic delamination current which occurs after 16 h. One alternative explanation for the increase of potential in the delaminated area would be a corresponding shift in the potential observed at the defect, for example in the case of corrosion product accumulation. However, given both the defect geometry, and the amount of electrolyte contained within the defect, it is unlikely that significant shifts in the defect potential would occur after 100 h.

It has previously been shown that potentials in the near near-defect delaminated region can become "pinned" by galvanic coupling to the defect.[10] Thus, when the process of cathodic delamination on zinc was arrested by switching the experimental atmosphere to nitrogen, E_{corr} values beneath the delaminated coating close to the defect were not found to change significantly.[10] In contrast, E_{corr} values close to the delamination front (and far from the defect) were found to change in a manner determined by the zinc/zincate equilibrium (as is assumed in the current paper). Furthermore, near-defect potential "pinning" is not observed under circumstances where coupling to the defect is diminished by the underfilm precipitation of corrosion products.[31] The SKP derived E_{corr} profiles in Fig. 9 show no evidence of potential "pinning" to the defect after cathodic disbondment has ceased and on this basis the assumption that the subsequent time-dependent evolution of underfilm E_{corr} results from a time-dependent pH increase would seem to be a reasonable one.

100 nm *Wedge;* Experiments were completed on three different 600 nm wedge samples and cathodic disbondment was not observed over the Mg bearing portions in any of the cases. The analysis of time-dependent SKP E_{corr} data was therefore repeated for different ZM layer thicknesses between 0 and 100 nm initial Mg (Table I).

Figure 11 shows the time dependent $E_{corr}(x)$ profiles obtained for line 7 (25 nm Mg). The profiles shown in Fig. 11 are somewhat noisy as a result of the nature of the inter-diffused ZM layer, and

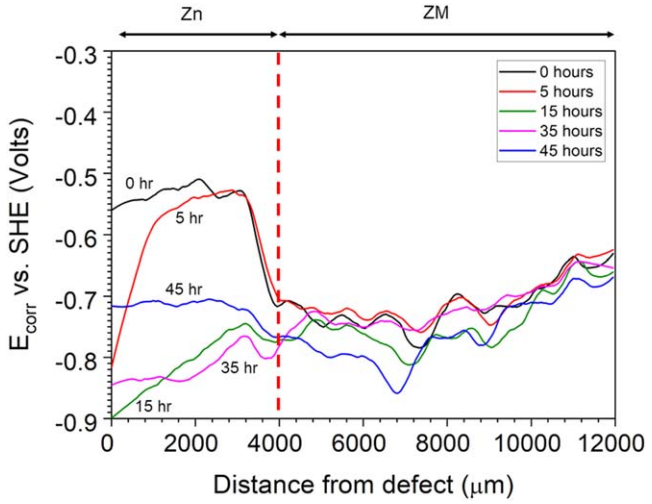

Figure 11. SKP derived E_{corr} as a function of distance from defect *(x)* profiles for the delamination of a PVB model coating from a ZM wedge coated HDG substrate after initiation using a 0.86 M NaCl electrolyte. The profile is taken from portions of the sample surface where the initial (pre-interdiffused) Mg layer thickness was 25 nm.

have been smoothed to allow for easy identification of the delamination front. The accurate determination of the delaminated distance was confirmed by visual inspection of the sample following removal from the SKP. In Fig. 11 E_{intact} values are more variable over the ZM portion of the sample (~ -0.55 to ~ -0.35 V vs SHE) than in Fig. 9, suggesting greater heterogeneity in the thinner ZM layer. Once again the delamination front propagates from left to right over the unmodified Zn portion of the sample and comes to a stop at the edge of the ZM region. Once delamination has ceased, E_{corr} over the unmodified Zn surface increases with time and reaches ~ -0.7 V vs SHE after 45 h. A slight but clear decrease in potential is observed within the ZM region ($\sim$7000 μm away from the defect) after $\sim$45 h. However, upon inspecting the sample following experimentation, it was confirmed that there was no evidence of mechanical coating disbondment and any potential drop shown cannot be attributed to the occurrence of a cathodic disbondment mechanism. In comparison to Fig. 9, the potential difference between the intact and defect

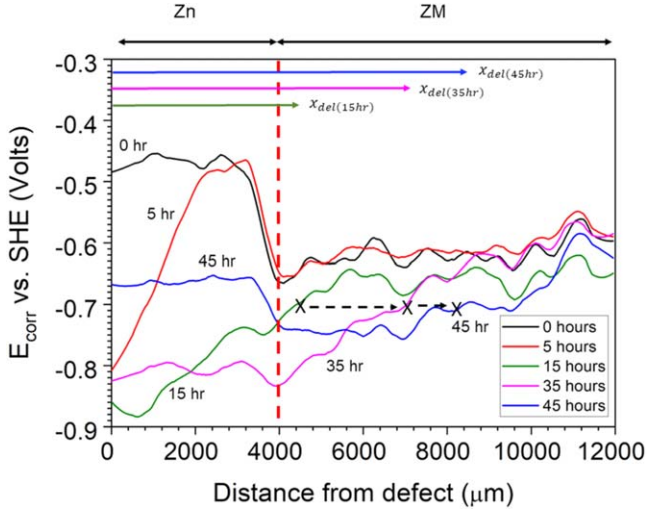

Figure 12. SKP derived E_{corr} as a function of distance from defect *(x)* profiles for the delamination of a PVB model coating from a ZM wedge coated HDG substrate after initiation using a 0.86 M NaCl electrolyte. The profile is taken from portions of the sample surface where the initial (pre-interdiffused) Mg layer thickness was 16 nm.

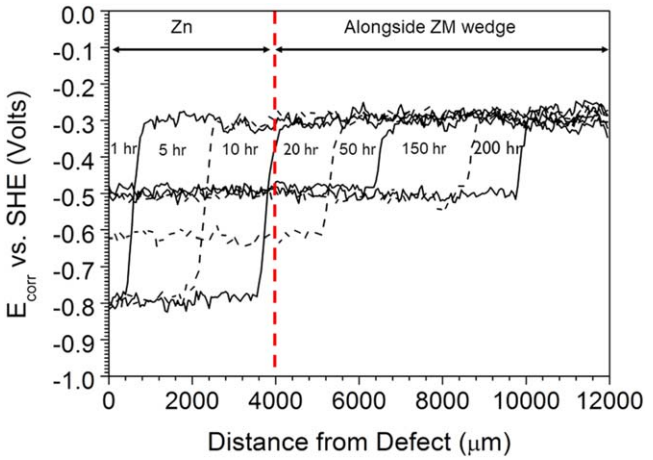

Figure 13. SKP derived E_{corr} as a function of distance from defect *(x)* profiles for the delamination of a PVB model coating from a ZM wedge coated HDG substrate after initiation using a 0.86 M NaCl electrolyte. The profile is taken from portions of the sample surface where the initial (pre-interdiffused) Mg layer thickness was 0 nm (Mg free line).

region is significantly reduced and only limited galvanic polarity (required to prevent cathodic delamination) is observed. In Fig. 12 the potential difference between the intact ZM portion (16 nm Mg) and the defect is further reduced (compared to Fig. 11) and the delamination front continues to propagate from the unmodified Zn portion of the sample and over the ZM region.

Figure 13 shows the time-dependent $E_{corr}(x)$ data derived from the Mg-free "corridor" region of 600 nm ZM wedge sample which was intended to provide an internal control for the combinatorial metrology. Initially $E_{corr}(x)$ profiles become established and evolve in a manner identical with the PVB coated HDG (Fig. 8) for which E_{intact} is initially ~ -0.3 V vs SHE and E_{corr} falls to ~ -0.7 V vs SHE in the delaminated region. The delamination front moves from left to right until it reaches a position which is parallel with the edge of the ZM coated portion of the sample. At this point the delamination front continues to advance unimpeded (as shown in Fig. 13). However, E_{corr} values in the delaminated region now start to increase in a similar fashion to in Figs. 11 and 12 and reach ~ -0.5 V vs SHE in the defect area after 20 h. Once the PVB coating has delaminated and an electrolyte layer has ingressed, a lateral diffusion of electrolyte ions becomes possible. That is to say, ions (such as OH^- and H^+), dissolved in the electrolyte layer, can diffuse in a direction normal to the direction of the delamination. Furthermore, because of the Grotthus mechanism,[32] the diffusion of OH^-/H^+ is expected to be relatively fast. Consequently, pH values in the delaminated region will tend to become uniformized in the direction normal to delamination. This will in turn produce a uniformization of underfilm E_{corr}.

Figure 14 shows x_{del} plotted as a function of the associated $t_{del}^{1/2}$ in the case that the Mg layer thickness (pre-interdiffusion) varies between 0 and 25 nm. In the case of 7 nm and 16 nm thick coatings the delamination rate is comparable to that obtained in the absence of the ZM layer. This finding suggests that very limited amount (incomplete) IM is formed. In both cases, delamination kinetics are parabolic and follow Eq. 12. For a thickness of 25 nm, cathodic delamination is suppressed upon reaching the ZM layer. This means that only very small amounts of Mg are necessary to prevent the cathodic delamination of coatings from galvanized steel. The complexity of the wedge experiments made it difficult to make repeat measurements for the 100 nm ZM wedge sample. However, delamination was not observed in the case that the Mg layer thickness was reduced to 31 nm (as was the case for line 9 of the three 600 nm wedge samples tested) or in the case that the layer thickness was decreased to 26 nm (as was the case for the 100 nm wedge sample). For all four wedge coatings, cathodic delamination

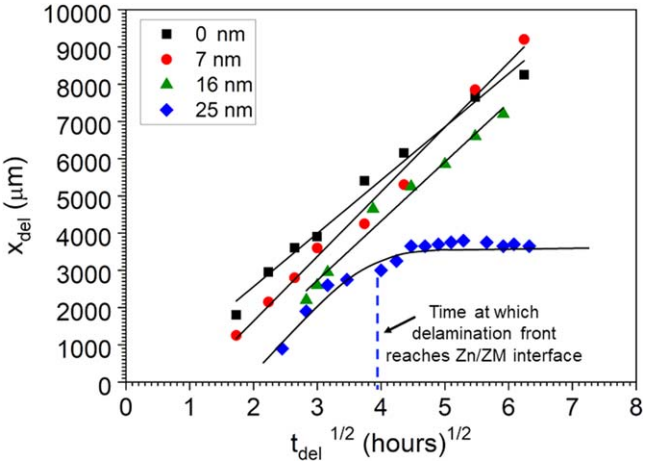

Figure 14. Plots of delamination distance (x_{del}) vs t for the disbondment of a model PVB coating from a ZM PVD wedge on HDG.

was therefore suppressed by ∼25–35 nm thick Mg layers and it would seem reasonable to propose that any error would result in a ∼ 10 nm difference in the thickness of Mg needed to prevent cathodic delamination.

The above findings have a number of implications;

i) The similarity of x_{del} vs time kinetics for the HDG Zn and the Zn corridor (internal control) experiments support the validity of the combinatorial approach. That is to say, there is no evidence that the lateral proximity of a compositionally different surface interferes with local rates of PVB coating delamination.
ii) Figures 8 and 14 suggest that E_{corr} values in the delaminated region do not significantly influence delamination rate on Zn. However, it must be borne in mind that delamination kinetics on Zn are parabolic and therefore controlled by ionic mass transport between the defect and the delamination front rather than any activation-controlled process at the front itself.[7]

Conclusion

Work has been completed to show that it is possible to produce a Mg/Zn alloy combinatorial library on a single substrate through physical vapour deposition (PVD) of a Mg "wedge", followed by thermal treatment to promote interdiffusion with the HDG Zn substrate. A rapid, parallel characterisation of the alloy library, with respect to resistance to corrosion driven cathodic delamination, can then be completed using SKP.

- A combination of SEM, GDOES and XRD were used to show that thermal heat treatment resulted in the formation of a Zn-Mg coating consisting principally of a Mg_2Zn_{11} layer, with the possible superposition of an $MgZn_2$ layer at higher Mg coating weights.
- The presence of surface IMs produced a depression in Volta potential consistent with Mg_2Zn_{11} exhibiting a work function of 3.6 eV.
- When Volta potentials are converted into electrochemical potentials (E_{corr}) by calibration, the local E_{intact} (which, in the context of an intact non conducting PVB coated metal, reflects the open circuit potential of the oxide-covered metal substrate[24]) values varied with the initial (pre inter-diffusion) Mg layer thickness. Mg free, Zn (HDG) portions of the sample exhibited E_{intact} of ∼ − 0.3 V vs SHE. The E_{intact} value remained constant at −1.0 V vs SHE for Mg thickness values ⩾100 nm and ⩽400 nm and decreased to −1.4 V vs SHE for Mg thickness values ⩾400 nm.
- A greater variation in E_{intact} values with thickness was observed in the case that the initial Mg layer thickness <100 nm. The potential decreased almost linearly from −0.3 V vs SHE to −0.6 V vs SHE for thicknesses between 0 nm and 70 nm.
- The susceptibility of ZnMg IMs (formed by interdiffusion), to corrosion driven cathodic delamination is strongly dependent upon (pre-interdiffusion) Mg coating weight. A (pre-interdiffusion) thickness of as little as 25 nm is sufficient to arrest actively propagating cathodic delamination on Zn (HDG).
- There is no evidence that any "cross-talk," which may occur between regions of dissimilar Mg coating weight, effects the cathodic delamination rate.
- The findings are entirely consistent with the theory advanced by Rohwerder et al.[1–4,33] That is to say that, as with pure $MgZn_2$, the effect of the Mg_2Zn_{11} formed is to reduce the overpotential between the defect and delamination front such that the driving force for cation insertion at the delamination zone is diminished or removed altogether. The implication here is that it is the presence of Mg that results in the resistance to corrosion driven cathodic delamination, as opposed to the presence of a particular Mg intermetallic.
- The finding that cathodic delamination is suppressed in cases when a reduction in overpotential between the defect and delamination front is observed, supports the hypothesis that the potential gradient can be adjusted (to zero) by changing the composition of the magnesium–zinc oxide at the surface of coatings. This in turn reduces the driving force for ion migration and galvanic coupling such as to suppress corrosion driven coating delamination.[1]
- It is significant that the presence of Mg_2Zn_{11} alone would appear sufficient to strongly inhibit cathodic disbondment and the presence of $MgZn_2$ (in quantities detectable by glancing angle XRD) is not required.

Acknowledgments

The authors would like to thank EPSRC and Tata Steel UK for funding this work.

References

1. R. Hausbrand, M. Stratmann, and M. Rohwerder, *Corros. Sci.*, **51**, 2107 (2009).
2. R. Hausbrand, M. Stratmann, and M. Rohwerder, *Steel Res. Int.*, **74**, 453 (2003).
3. R. Hausbrand, M. Stratmann, and M. Rohwerder, *J. Electrochem. Soc.*, **155**, C369 (2008).
4. A. Vimalanandan., A. Bashir, and M. Rohwerder, *Mater. Corros.*, **65**, 392 (2014).
5. G. Williams and H. N. McMurray, "Underfilm/coating corrosion." in *Shreir's Corrosion*, ed. B. R. A. Cottis et al. (Elsevier, Amsterdam) p. 988 (2009).
6. A. Leng., H. Streckel, and M. Stratmann, *Corros. Sci.*, **41**, 547 (1999).
7. A. Leng., H. Streckel, and M. Stratmann, *Corros. Sci.*, **41**, 579 (1999).
8. G. Williams and H. N. McMurray, *J. Electrochem. Soc.*, **148**, B377 (2001).
9. W. Furbeth and M. Stratmann, *Fresenius' J. Anal. Chem.*, **353**, 337 (1995).
10. W. Furbeth and M. Stratmann, *Corros. Sci.*, **43**, 207 (2001).
11. W. Chen, Q. Liu, Q. Liu, L. Zhu, and L. Wang, *J. Alloys Compd.*, **459**, 261 (2008).
12. A. Kafizas. and I. P. Parkin, *Chem. Soc. Rev.*, **41**, 738 (2011).
13. M. L. Green, I. Takeuchi, and J. R. Hattrick-Simpers, *J. Appl. Phys.*, **113**, 231101 (2013).
14. T. Prosek, D. Persson, J. Stoulil, and D. Thierry, *Corros. Sci.*, **86**, 231 (2014).
15. G. J. Reynolds, Z. S. Barrett, H. N. McMurray, and G. Williams, *Corros. Sci.*, **70**, 82 (2016).
16. C. Stromberg, P. Thissen, I. Klueppel, N. Fink, and G. Grundmeier, *Electrochim. Acta*, **52**, 804 (2006).
17. B. Schuhmacher., C. Schwerdt, U. Seyfert, and O. Zimmer, *Surf. Coat. Technol.*, **163**, 703 (2003).
18. B. Navinšek., P. Panjan, and I. Milošev, *Surf. Coat. Technol.*, **116–119**, 476 (1999).
19. J. L. Davies, cf Glover, J. Van de Langkruis, E. Zoestbergen, and G. Williams, *Corros. Sci.*, **100**, 607 (2015).
20. N. C. Hosking, M. A. Ström, P. H. Shipway, and C. D. Rudd, *Corros. Sci.*, **49**, 3669 (2007).
21. B. Scheffel., C. Metzner, T. Modes, O. Zywitzki, and H. Morgner, "Functional and decorative coatings onto stainless steel sheets and strips deposited by high-rate physical vapour deposition." 7th European Stainless Steel Conf.: Science and Market, Proc. (2011).
22. O. Zywitzki, T. Modes, B. Scheffel, and C. Metzner, *Practical Metall.*, **49**, 210 (2012).
23. I. Suzuki., in *Corrosion-Resistant Coatings Technology* (CRC Press, Boca Raton, FL) (1989).

24. M. Stratmann, R. Feser, and A. Leng, *Electrochim. Acta*, **39**, 1207 (1994).
25. A. Leng., A. H. Streckel, K. Hoffman, and M. Stratmann, *Corros. Sci.*, **41**, 599 (1999).
26. A. Nazarov. and D. Thierry Dominique, *Front. Mater.*, **6**, 192 (2019).
27. H. N. McMurray and G. Williams, *J. Appl. Phys.*, **91**, 1673 (2002).
28. M. Morishita, H. Yamamoto, S. Shikada, M. Kusumoto, and Y. Matsumoto, *Mater. Trans.*, **51**, 1705 (2010).
29. H. B. Michaelson, *J. Appl. Phys.*, **48**, 4729 (1977).
30. E. A. Mechtly, "Properties of materials." in *Reference Data for Engineers*, ed. W. M. Middleton and M. E. Van Valkenburg (Newnes, Boston, MA) 9th ed. (2002).
31. A. Merz., M. Uebel, and M. Rohwerder, *J. Electrochem. Soc.*, **166**, C304 (2019).
32. C. J. T. de Grotthuss, *Ann. Chim. Phys., LVIII*, 54 (1806).
33. V. Shkirskiy, M. Uebel, A. Maltseva, G. Lefèvre, P. Volovitch, and M. Rohwerder, *npj Mater. Degrad.*, **3**, 1 (2019).